nature photonics

LETTERS

PUBLISHED ONLINE: 21 OCTOBER 2012 | DOI: 10.1038/NPHOTON.2012.260

Non-polarizing broadband multilayer reflectors in fish

T. M. Jordan[1,2], J. C. Partridge[1] and N. W. Roberts[1]*

Dielectric multilayer reflectors that are non-polarizing are an important class of optical device and have numerous applications within optical fibres[1], dielectric waveguides[2] and light-emitting diodes[3]. Here, we report analyses of a biological non-polarizing optical mechanism found in the broadband guanine-cytoplasm 'silver' multilayer reflectors of three species of fish. Present in the fish stratum argenteum are two populations of birefringent guanine crystal, with their optical axes either parallel to the long axis of the crystal or perpendicular to the plane of the crystal, respectively. This arrangement neutralizes the polarization of reflection as a result of the different interfacial Brewster's angles of each population. The fish reflective mechanism is distinct from existing non-polarizing mirror designs[4–7] in that, importantly, there is no refractive index contrast between the low-index layers in the reflector and the external environment. This mechanism could be readily manufactured and exploited in synthetic optical devices.

Multilayer reflectors occur extensively in nature. They are used by animals to create iridescent signals for communication[8], crypsis for camouflage[9] and as reflectors to increase low light sensitivity in many eyes[10]. Silvery reflections from fish are produced by multilayer 'stacks' of high-refractive-index guanine crystals separated by low-refractive-index cytoplasm gaps[11]. Many fish have two separate forms of these stacks: (i) those in the stratum argenteum, a subdermal layer of the skin, and (ii) those that lie on the inner surface of the scales[12,13]. These reflecting structures provide cryptic camouflage in the near-axially symmetric underwater light field, with reflections matching the intensity of rays from behind[13]. For optimal concealment, the reflecting structures must produce both spectrally broadband and high-percentage, non-polarizing reflectivity over all angles of incidence. Non-polarizing reflectors are advantageous as they are not subject to a reduction in overall reflectivity as angles of incidence approach Brewster's angle. Multilayer mechanisms capable of producing broadband reflectivity in fish are well understood[14,15], with the random layer thickness variation in the subdermis reported by McKenzie *et al.*[15] providing the biological analogue of disordered synthetic dielectric mirrors[16]. Past experimental studies have suggested that reflections from fish are of low polarization[17,18]. However, this property of reflection has never been explained and all existing optical models[10,15,19,20] predict full Fresnel polarization at Brewster's angle.

Initially, we used reflectance spectrophotometry to characterize the polarization dependence of the reflectivity from two species of fish, *Clupea harengus* (Atlantic herring) and *Sardina pilchardus* (European sardine); see Methods for details of the experimental set-up. We measured the specular component of reflectivity for light polarized perpendicular and parallel to the plane of incidence, $R_\sigma(\lambda,\theta)$ and $R_\pi(\lambda,\theta)$, and calculated the degree of polarization:

$$d(\lambda,\theta) = \left(\frac{R_\sigma - R_\pi}{R_\sigma + R_\pi}\right) \quad (1)$$

for reflected light. In accordance with previous studies[17,18], the polarization by reflection is very different to a Fresnel dielectric with low polarization across all wavelengths and at all angles of incidence. Measurements of $d(\theta)$ at $\lambda = 600$ nm about the azimuthal (dorsoventral) and latitudinal (rostrocaudal) axes of illumination for *C. harengus* are shown in Fig. 1a. We estimated the percentage error of the experimental arrangement for an ideal flat sample to be ~1% by measuring $d(\theta)$ for a glass microscope slide and comparing our measured values to theoretical values for double-image Fresnel equations[21] (Fig. 1a). Both fish data sets have maximum polarization values of ~0.35 at $\theta = 60^\circ$, suggesting that the polarization behaviour is near-independent of axis of rotation. At all angles of incidence the reflection spectra are broad bandwidth with no gaps in the high reflectance region (Fig. 1b,c). Measurements from samples of *S. pilchardus* exhibit very similar generic reflection and polarization behaviour (Supplementary Fig. S1).

All previous multilayer models of fish reflectors[10,15,19,20] assume that the crystals behave as optically isotropic layers with a refractive index of ~1.83. These crystals, however, are in fact highly birefringent, being a mixture of pure guanine and hypoxanthine, which have refractive indices of (1.93, 1.91, 1.47) and (1.85, 1.78, 1.42)[22]. The guanine–hypoxanthine ratio varies between fish, with the crystals found in *C. harengus* reported to have refractive index values of (1.85, 1.81, 1.46)[13,22]. It has conventionally been thought that the optical axes of the crystals all have a common orientation in the multilayer structure, with the low refractive index value aligned with the short axis of the crystal and the direction of stacking (by convention, the *z*-axis)[13]. However, it has recently been demonstrated that the relative axial growth rate of crystals in fish is subject to biological control mechanisms, changing the optic axis of the crystal[23]. This motivated us to re-examine the optical properties of individual guanine crystals from the stratum argenteum and the inner surface of teleost scales. We used a digital holographic transmission microscope to measure the ratio of the refractive indices along the two planar crystal axes (see Methods for a description of this technique).

In three species of clupeid teleost we identified two distinct populations of guanine crystals that are morphologically identical but have different optical properties. In the stratum argenteum there are both *Type 1* and *Type 2* crystals, which have planar refractive index ratios of ~1.025 and ~1.250, respectively (Fig. 2 and Supplementary Fig. S2). Under the scales, only *Type 1* crystals exist, but these crystals have a different lower-aspect-ratio morphology compared with the crystals from the argenteum. These differences in shape have been reported previously by

[1]School of Biological Sciences, Woodland Road, University of Bristol, Bristol BS8 1UG, UK, [2]Bristol Centre for Complexity Sciences, University of Bristol, Queen's Building, University Walk, Bristol BS8 1TR, UK. *e-mail: nicholas.roberts@bristol.ac.uk

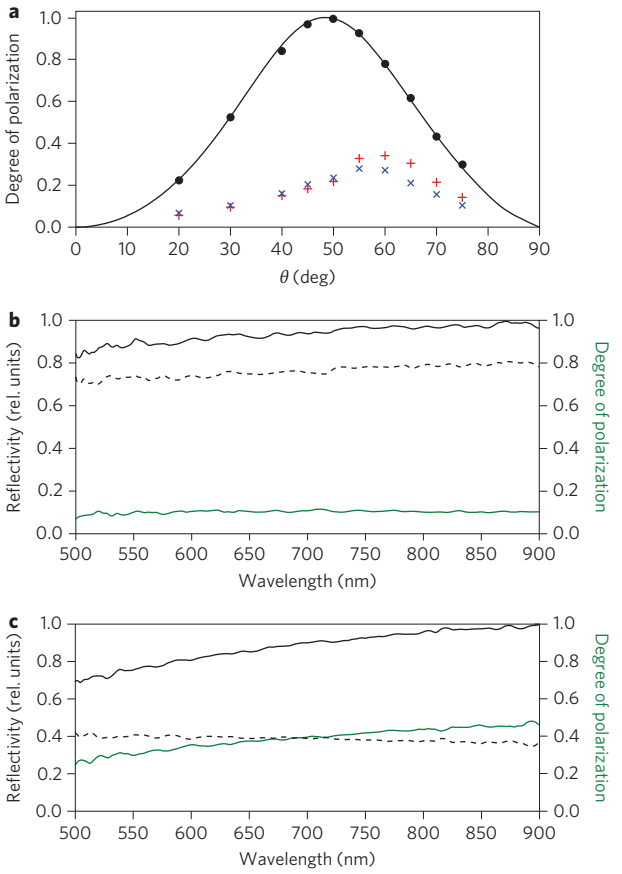

Figure 1 | Optical reflectivity measurements. a, Measurements of the degree of polarization $d(\theta)$ at $\lambda = 600$ nm for azimuthal (dorsoventral; red cardinal crosses) and latitudinal angles of illumination (rostrocaudal; blue obligue crosses) from *Clupea harengus*. Black solid circles and black line represent a positive control and are experimental data and a theoretical curve for a double surface Fresnel reflection (front and back reflection) from a glass microscope slide with a refractive index of 1.50, in air. **b**,**c**, Reflection and degree of polarization spectra at 30° (**b**) and 60° (**c**). In **b** and **c** the black solid line is $R_\sigma(\lambda)$, the black dashed line is $R_\pi(\lambda)$ and the green solid line is $d(\lambda)$.

Denton and Nicol[12] and Denton[13]. It is also worth noting here that although the opercula (gill covers) of both fish species have no scales, the skin contains both physical shapes of the *Type 1* crystals as well as *Type 2* crystals. In agreement with the literature[13,22], our measurements of *Type 1* crystals imply that the low refractive index value is aligned with the *z*-axis. The measurements for *Type 2* crystals are very different from the optical properties reported to date and imply that the low refractive index value is orientated in the *x*–*y* plane.

We used the anisotropic 4 × 4 matrix technique[24,25] to calculate the reflectivity of a guanine–cytoplasm multilayer containing these two populations of crystals (details of the theory are provided in the Methods). In this model, the weakly biaxial crystals were approximated as uniaxial birefringent planar layers with ordinary refractive index $n_o = 1.83$ and extraordinary refractive index $n_e = 1.46$. A schematic example of the modelled structure is presented in Fig. 3a, illustrating the two populations of guanine crystals and their associated refractive indices. Each crystal layer was randomly assigned a 'population state', with *Type 1* crystals having mixing ratio f and *Type 2* crystals having mixing ratio $(1–f)$. Refractive index vectors for each population are given by

$$\textit{Type 1} \qquad \mathbf{n}_g = (n_o, n_o, n_e) \tag{2}$$

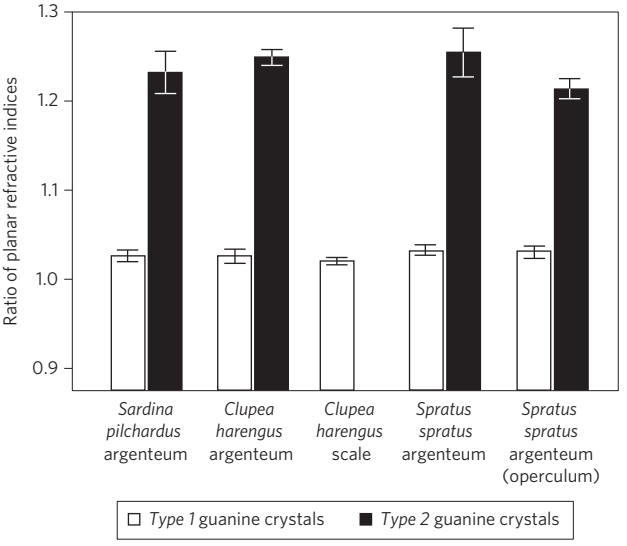

Figure 2 | Refractive index ratios of guanine crystals. Measurements (mean ± s.d.) of the planar refractive index ratios in *Type 1* and *Type 2* guanine crystals in *Clupea harengus*, *Sardina pilchardus* and *Spratus spratus*. The multilayers under the scales of *C. harengus* contained only *Type 1* crystals.

$$\textit{Type 2} \qquad \mathbf{n}_g = \left(\sqrt{\cos^2(\phi)n_o^2 + \sin^2(\phi)n_e^2}, \sqrt{\cos^2(\phi)n_e^2 + \sin^2(\phi)n_o^2}, n_o\right) \tag{3}$$

where ϕ is a uniformly distributed random variable on the interval $[0, \pi]$, and n_o and n_e are the ordinary and extraordinary refractive indices, respectively. The isotropic cytoplasm layers and the external environment (water) both have a refractive index of 1.33 (ref. 19). The broad bandwidth of our reflection spectra are best accounted for by assuming that the thicknesses of the guanine and cytoplasm layers can be modelled as uniformly distributed random variables[15]. Our model used a thickness sampling interval of [55, 110] nm for the thickness of the guanine crystals[14], with the bounds for cytoplasm layer thicknesses allowed to vary freely over physiologically plausible values[15]. The in *x*–*y*-plane symmetry of the reflection spectra in Fig. 1a indicates rotational invariance of the macroscopic structure, so we averaged over 500 multilayer structures to account for variation at the microscopic scale (as modelled).

Our optical model predicts that multilayers with only *Type 1* crystals ($f = 1$) have a fully polarizing Brewster's angle at 67° (black line in Fig. 3b). This polarization behaviour is anticipated by the anisotropic interfacial reflection coefficients for each individual layer[26], which have a Brewster's angle θ_B given by the relation

$$\tan(\theta_B) = \left(\frac{n_{g,z}}{n_c}\right)\sqrt{\left(\frac{n_c^2 - n_{g,x}^2}{n_c^2 - n_{g,z}^2}\right)} \tag{4}$$

where subscripts *c* and *g* indicate cytoplasm or guanine and subscripts *x* and *z* indicate Cartesian components[27]. This is standard Fresnel behaviour and is similar to that occurring if the crystals are assumed to be isotropic, in which case equation (4) reduces to $\tan(\theta_B) = (n_g/n_c)$ and Brewster's angle is at 53° (blue line in Fig. 3b). However, when there are two populations of crystal present in the multilayer structure, low-polarization reflections over all angles of incidence can occur. We applied a parametric grid search to the experimental data from *C. harengus* in Fig. 1a,

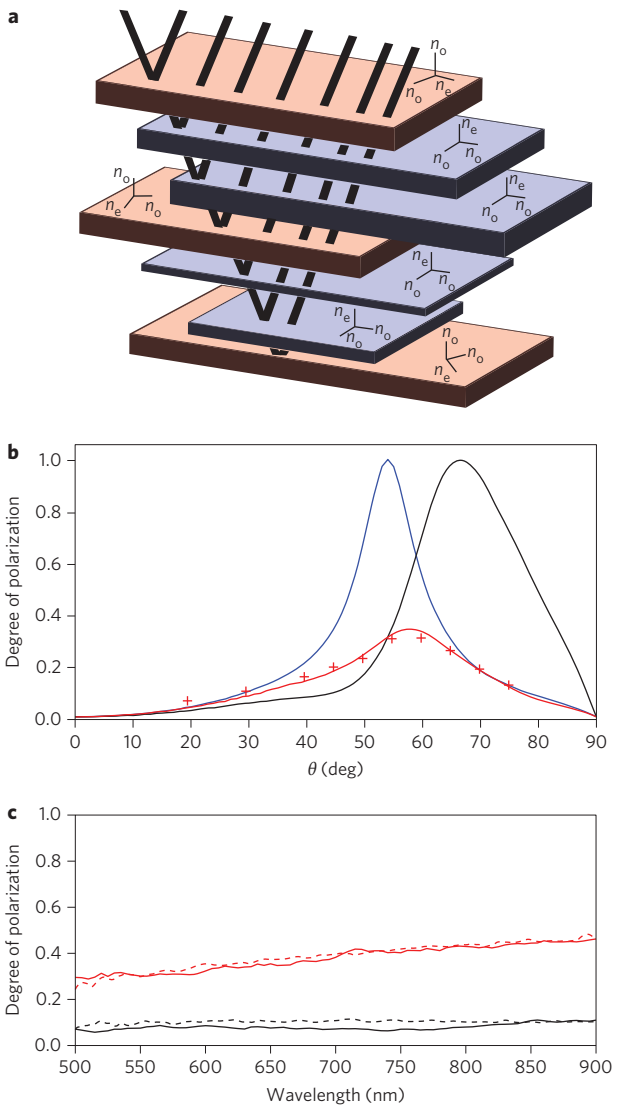

Figure 3 | Optical structure, modelling and parametric fit to experimental data. a, Schematic illustrating the multilayer model used and the two populations of guanine crystals: *Type 1* crystals (purple) and *Type 2* crystals (orange). The orientation of the principle refractive indices' coordinate axes in each crystal layer are indicated. **b**, Simulations of the degree of polarization $d(\theta)$ at different angles of incidence θ and at $\lambda = 600$ nm for three classes of multilayer model, including a parametric fit to experimental data from *Clupea harengus*. The black line is for a multilayer of *Type 1* crystals ($f = 1$), the blue line is for isotropic crystals ($n_o = n_e = 1.83$), and the solid red line is a parametric best fit for a mixture of *Type 1* and *Type 2* crystals with $f = 0.75$. The red crosses are the mean of the azimuthal and latitudinal data from Fig. 1a. Our model explained 95% of the variation in the data, assessed by the R^2 from linear regression. There was no systematic difference between model and data (mean pairwise difference and s.d. = 0.0044 ± 0.0132, $t = 0.7512$, d.f. = 9, $P = 0.472$). The best fit parameters are $N = 37$ crystal layers in each multilayer structure, with sampling intervals for guanine and cytoplasm thicknesses of [55, 110] nm and [30, 300] nm, respectively. **c**, Simulated degree of polarization $d(\lambda)$ for the parametric best fit in **b** (solid black line $\theta = 30^\circ$ and solid red line $\theta = 60^\circ$) and experimental $d(\lambda)$ from *C. harengus* (dashed black line $\theta = 30^\circ$ and dashed red line $\theta = 60^\circ$) as in Fig. 1b,c.

allowing for N, f and the sampling interval bounds upon the cytoplasm thickness to vary. We found $f = 0.75$, $N = 37$ and thickness bounds of [30, 300] nm to give the best parametric fit. Our model explained 95% of the variation in the data, assessed by the R^2 from linear regression. There was no systematic difference between model and data (mean pairwise difference and standard deviation (s.d.) = 0.0044 ± 0.0132, $t = 0.7512$, degrees of freedom (d.f.) = 9, $P = 0.472$) (red solid in line in Fig. 3b; see Supplementary Fig. S1 for a similar analysis of data from *S. pilchardus*). The values of N for the parametric fits for both fish are in excellent agreement with past histological surveys[14]. Figure 3c further shows the similar agreement between the experiment and modelled results for both $\theta = 30^\circ$ (black lines) and $\theta = 60^\circ$ (red lines) as a function of wavelength. The reason underlying this non-trivial polarization behaviour is the different interfacial Brewster's angles between the isotropic layers and either the *Type 1* crystals or the different orientations in the plane of the *Type 2* crystals, which can lie anywhere in the interval $[33^\circ, 53^\circ]$ (equation (4)). One further possible explanation for this polarization behaviour that has been considered is polarization mode mixing in the multilayer structure. With changes in polarization occurring due to the changing orientation of the optical axes of the birefringent layers, a contribution might always exist perpendicular to the plane of incidence and therefore be reflected. However, we have both experimentally measured and theoretically calculated (using the best-fit parameters above) both $R_{\pi\sigma}$ and $R_{\sigma\pi}$ for *C. harengus* (Supplementary Fig. S3). In both the experimental measurements and optical modelling, the contributions of these cross terms are extremely small and cannot account for the polarization response of the structure.

Clearly, the real biological multilayer reflectors of *C. harengus* and *S. pilchardus* are weakly polarizing. However, by increasing the number of layers in the multilayer structure, the optical mechanism can produce true polarization-neutral reflections. This property is demonstrated in Fig. 4a, which indicates a monotonic decrease in the degree of maximum polarization with increasing N, and Fig. 4b, which shows a reflectance band for both σ and π polarizations approaching 100% reflectivity at $\theta = 60^\circ$ (which is approximately the angle of highest polarization). Natural photonic structures are proving to be of inspiration for optical technologies[28], with the organization of birefringent materials in animals leading to the fabrication of novel biomimetic devices[29,30]. Common to all existing non-polarizing mirror designs is the use of a refractive-index contrast between the low-index layers in the reflector and the external environment (for example, refs 4–7), which enables the reflector to be screened from angles of incidence where polarization occurs. The fish reflective mechanism places no such restriction, and is instead dependent on having both birefringent layers with different interfacial Brewster's angles and there being a high variation in the optical thickness of the layers. Highly birefringent polymers with similar refractive indices to the fish have already been used in multilayer mirror designs[26], although these studies do not discuss the production of non-polarized reflections through two different populations of birefringent layers. The polarization properties of a biomimetic design that replaces the two populations of crystals with two uniaxially birefringent populations of layers with refractive indices (1.83, 1.83, 1.33) and (1.33, 1.33, 1.83) are illustrated in Fig. 4c,d. This biomimetic design captures the essential physics of the fish reflective mechanism, but improves the efficiency of polarization neutralization by maximizing the disparity between the interfacial Brewster's angles of the two populations (equation (4)). It is important to be clear that the mechanism of polarization-neutral reflections described here is radically different from that of photonic-bandgap based non-polarizing mirrors. Unlike existing non-polarizing reflectors, the biomimetic design permits the environmental media and low-index layers to be made from the same material, and would provide an advantage in applications where the thermal and mechanical properties of the reflector benefit from being constructed with the same material externally and within the structure.

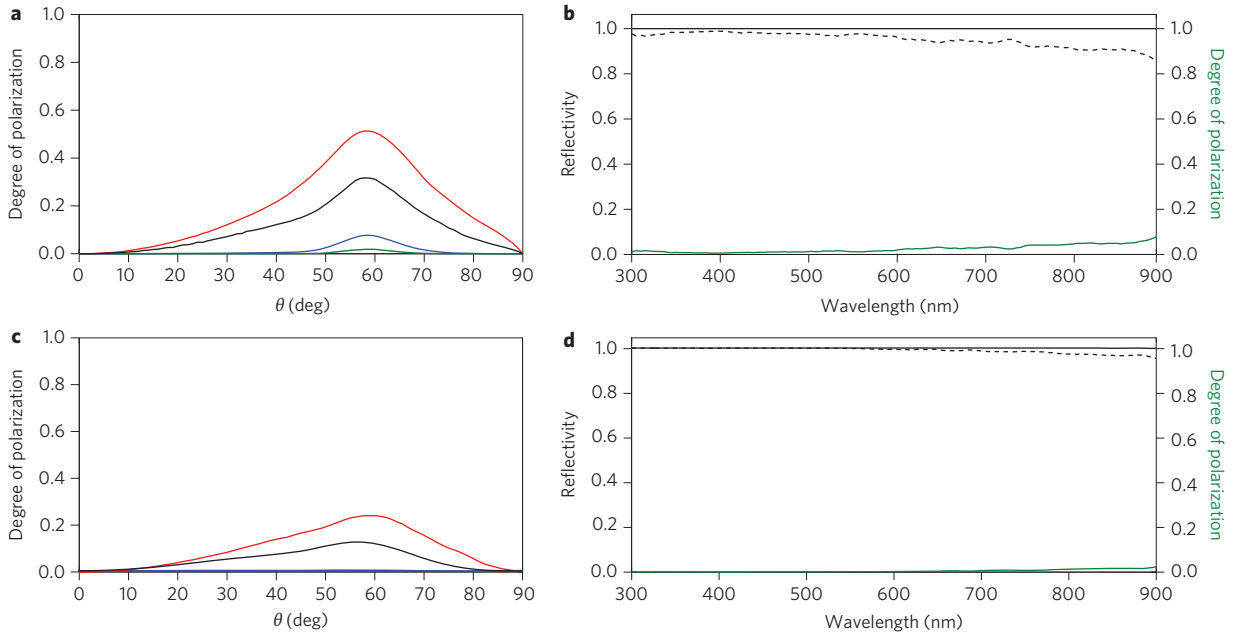

Figure 4 | A biologically inspired mechanism of polarization-neutral reflection. a–d, Simulated degree of polarization $d(\theta)$ at different angles of incidence θ and $\lambda = 600$ nm for $N = 20$, 40, 200, 400 crystal layers (red, black, blue and green solid lines, respectively) and accompanying reflection and polarization spectra at 60° for the fish reflective structure (**a**,**b**) and a biomimetic design (**c**,**d**) with two uniaxial populations of layers with refractive indices given by (1.83,1.83,1.33) and (1.33,1.33,1.83). $N = 400$ in **b** and $N = 200$ in **c**. The black solid line is $R_\sigma(\lambda)$, the black dashed line is $R_\pi(\lambda)$ and the green solid line is $d(\lambda)$. In all plots the layer thicknesses are sampled from uniform distributions on the intervals [55, 110] nm for the birefringent layers and [30, 300] nm for the isotropic layers, with $f = 0.75$ and the (1.83, 1.83, 1.33) layers being defined as *Type 1* in the biomimetic design.

In the context of an animal's visual ecology, to perfectly background-match an axially symmetric light field over all angles of incidence, any vertical dielectric reflector must produce non-polarizing broadband reflections, as well as having high reflectivity. By producing a high degree of polarization neutrality for reflections over all angles of incidence, the mechanism discovered in these species of fish ensures a greater total reflected intensity that more closely matches the open water background light field. Although previous works have emphasized how the spectral properties of biological multilayer structures arise and the relationship that this has to biological function[14,19], our study exposes the fact that, provided one of the constituent materials has high birefringence, polarization properties, as well as spectral properties, can play a role in their structural organization. It is an intriguing possibility that the selection of polarization properties in the biological reflectors examined in this work are a direct adaptation to better intensity-match the pelagic light environment. It is worth adding that several aquatic animals including fish, cephalopods and crustaceans have polarization vision[31,32]. In an axisymmetric light environment, a consequence of a non-polarizing mechanism of intensity-matching is that the reflector also matches the polarization of the background[33]. Finally, it is likely that birefringence is key to the optical properties of other animal multilayer reflectors. The optical properties of silver reflectors in certain cephalopods[34] and the polarizing guanine–cytoplasm structures in the tapeta of some spiders[35] both still require explanation.

Methods

Reflectance spectrophotometry. Thin areas of fish skin and underlying tissue ~3 mm in thickness and 30 × 30 mm^2 in size were taken from the vertical lateral flank of each animal and mounted on a black perspex slide. Data were recorded about the azimuthal (dorsoventral) and latitudinal (caudorostral) axes, with the latitudinal angle of incidence at 90° when viewing the fish from the ventral direction and the azimuthal angle of incidence at 90° when viewing the fish from its rostral end (0° being normal incidence to the tissue in both cases). The sample was placed in the centre of an optically clear, cylindrical, perspex tank filled with water, with the incident and reflected beams locally perpendicular to the tank surface. An Ocean Optics DH2000 halogen lamp was used as an illuminant, with an Ocean Optics QE65000 spectrometer used as a photon detector over a range of angles from 20° to 75°. Light from the lamp was directed onto the fish skin via fibre optic (Ocean Optics P600-2-UV/VIS), terminated with an Ocean Optics 74-UV lens (NA = 0.24), and reflected light was collected and directed to the spectrometer by an identical lens and fibre combination. The beam spot was 5 mm in diameter. The lenses were mounted on rotating arms, with the centre of rotation coincident and above the surface of the sample. Glan–Thompson achromatic polarizers were placed in the beam path before (all measurements) and after (when measuring the four polarization mode combinations, $R_{\pi\pi}$, $R_{\pi\sigma}$, $R_{\sigma\sigma}$ and $R_{\sigma\pi}$) the sample.

Digital holographic microscopy. We isolated the individual crystals using the methods described by Denton and Land[14]. We measured the phase retardation parallel and perpendicular to the long axis of the crystal (indicated by red and black arrows in Supplementary Fig. S2a,b) using a digital holographic microscope. A detailed description of the technique is set out by Colomb and colleagues[36]. We made six separate measurements of the phase retardation parallel and perpendicular to the long axis of each crystal, and used the two retardations to calculate the mean planar refractive index ratio. For each species (and sample area) we measured 20 crystals, calculating the mean and standard deviation of measurements (Fig. 2).

Optical modelling. The optical model assumes that the guanine–cytoplasm stack can be approximated as a planar stratified medium with alternating isotropic and uniaxial birefringent layers. The coordinate system was chosen so that the z-axis was aligned with the direction of stacking and the σ polarization was aligned with the y-axis. Each crystal layer was orientated at a random planar angle ϕ, where ϕ is a uniformly distributed random variable on $[0, \pi]$. The reflectivity was calculated using the 4 × 4 matrix method[24,25]. In this formulation, the dielectric properties of each crystal layer are represented by the differential propagation matrix Δ. For the *Type 1* crystals this is of the form

$$\Delta_1 = \begin{pmatrix} 0 & 1 - \dfrac{n_1^2 \sin(\theta_1)^2}{\epsilon_e} & 0 & 0 \\ \epsilon_o & 0 & 0 & 0 \\ 0 & 0 & 0 & 1 \\ 0 & 0 & \epsilon_o - n_1^2 \sin(\theta_1)^2 & 0 \end{pmatrix} \quad (5)$$

and for *Type 2* crystals it is of the form

$$\Delta_2 = \begin{pmatrix} 0 & 1-\frac{n_1^2\sin(\theta_1)^2}{\epsilon_o} & 0 & 0 \\ \epsilon_o\cos(\phi)^2+\epsilon_e\sin(\phi)^2 & 0 & \frac{1}{2}(\epsilon_o-\epsilon_e)\sin(2\phi) & 0 \\ 0 & 0 & 0 & 1 \\ \frac{1}{2}(\epsilon_o-\epsilon_e)\sin(2\phi) & 0 & \epsilon_o\sin(\phi)^2+\epsilon_e\cos(\phi)^2-n_1^2\sin(\theta_1)^2 & 0 \end{pmatrix} \quad (6)$$

where $\epsilon_o = n_o^2$, $\epsilon_e = n_e^2$ and n_1 is the refractive index of the incident medium, and θ_1 is the angle of incidence. The isotropic cytoplasm layers have the same form of Δ matrix as *Type 1* crystals, but with $\epsilon_c = n_1^2$ substituted for ϵ_o and ϵ_e, respectively. The transfer matrices for each layer were obtained using the procedure described by Azzam and Bashara[25]. The transfer matrix for the overall multilayer system was obtained by taking a matrix product over all layers, and reflectivity coefficients $R_\sigma = R_{\sigma\sigma} + R_{\sigma\pi}$ and $R_\pi = R_{\pi\pi} + R_{\pi\sigma}$ were then calculated using standard formulae[25]. To equate the microscopic structure with the bulk optical response and simulate a representative model, we sampled and averaged over 500 multilayer structures.

Received 17 February 2012; accepted 12 September 2012; published online 21 October 2012

References

1. Hart, S. D. *et al.* External reflection from omnidirectional dielectric mirror fibers. *Science* **296,** 510–513 (2002).
2. Yang, S. H., Cooper, M. L., Bandaru, P. R. & Mookherjea, S. Giant birefringence in multi-slotted silicon nanophotonic waveguides. *Opt. Express* **16,** 8306–8316 (2008).
3. Gessmann, T., Schubert, E. F., Graff, J. W., Streubel, K. & Karnutsch, C. Omnidirectional reflective contacts for light-emitting diodes. *IEEE Electron. Dev. Lett.* **24,** 683–685 (2003).
4. Fink, Y. A Dielectric omnidirectional reflector. *Science* **282,** 1679–1682 (1998).
5. Kaminska, K. & Robbie, K. Birefringent omnidirectional reflector. *Appl. Opt.* **43,** 1–7 (2004).
6. Han, P. & Wang, H. Criterion of omnidirectional reflection in a one-dimensional photonic heterostructure. *J. Opt. Soc. Am. B* **22,** 1571–1575 (2005).
7. Bria, D., Boudouti, E. H. E., Mir, A. & Akjouj, A. Omnidirectional optical mirror in a cladded-superlattice structure. *J. Appl. Phys.* **91,** 2569–2572 (2012).
8. Cronin, T., Chiou, T-H., Caldwell, R. & Roberts, N. Polarization signals in mantis shrimps. *Proc. SPIE* **7461,** 74610C (2009).
9. Jewell, S. A., Vukusic, P. & Roberts, N. W. Circularly polarized colour reflection from helicoidal structures in the beetle *Plusiotis boucardi*. *New J. Phys.* **9,** 99 (2007).
10. Land, M. F. & Nilsson, D-E. *Animal Eyes*, Oxford Animal Biology Series, 1st edn (Oxford Univ. Press, 2002).
11. Denton, E. J. & Nicol, J. Polarization of light reflected from the silvery exterior of the bleak, *Alburnus alburnus*. *J. Mar. Biol. Assoc. UK* **45,** 705–709 (1965).
12. Denton, E. J. & Nicol, J. A. C. Studies on reflexion of light from silvery surfaces of fishes, with special references to the bleak, *Alburnus alburnus*. *J. Mar. Biol. Assoc. UK* **45,** 683–703 (1965).
13. Denton, E. J. Review Lecture: On the organization of reflecting surfaces in some marine animals. *Phil. Trans. R. Soc. B* **258,** 285–313 (1970).
14. Denton, E. J. & Land, M. F. Mechanism of reflexion in silvery layers of fish and cephalopods. *Proc. R. Soc. B* **178,** 43–61 (1971).
15. McKenzie, D. R., Yin, Y. & McFall, W. D. Silvery fish skin as an example of a chaotic reflector. *Proc. R. Soc. A* **451,** 579–584 (1995).
16. Zhang, D., Li, Z., Hu, W. & Cheng, B. Broadband optical reflector—an application of light localization in one dimension. *Appl. Phys. Lett.* **67,** 2431–2432 (1995).
17. Denton, E. J. & Nicol, J. A. C. Reflexion of light by external surfaces of the herring, *Clupea harengus*. *J. Mar. Biol. Assoc. UK* **45,** 711–738 (1965).
18. Rowe, D. M. & Denton, E. J. The physical basis of reflective communication between fish, with special reference to the horse mackerel, *Trachurus trachurus*. *Proc. R. Soc. B* **352,** 531–549 (1997).
19. Land, M. F. The physics and biology of animal reflectors. *Prog. Biophys. Mol. Biol.* **24,** 75–106 (1972).
20. Levy-Lior, A. *et al.* Guanine-based biogenic photonic-crystal arrays in fish and spiders. *Adv. Funct. Mater.* **20,** 320–329 (2010).
21. Born, M. & Wolf, E. *Principles of Optics* 7th edn, 40–49 (Cambridge Univ. Press, 1999).
22. Greenstein, L. Nacreous pigments and their properties. *Proc. Sci. Sec. Toilet Goods Assoc.* **26,** 20–26 (1966).
23. Levy-Lior, A. *et al.* Biogenic guanine crystals from the skin of fish may be designed to enhance light reflectance. *Cryst. Growth Des.* **8,** 507–511 (2008).
24. Berreman, D. 4 × 4 matrix methods. *J. Opt. Soc. Am.* **62,** 502–510 (1972).
25. Azzam, R. M. & Bashara, N. M. *Ellipsometry and Polarized Light*, 269–363 (Elsevier, 1988).
26. Weber, M. F. Giant birefringent optics in multilayer polymer mirrors. *Science* **287,** 2451–2456 (2000).
27. Orfanidis, S. *Electromagnetic Waves and Antennas*; available at http://www.ece.rutgers.edu/orfanidi/ewa/ (accessed September 2012)
28. Vukusic, P. & Sambles, R. J. Photonic structures in biology. *Nature* **424,** 852–855 (2003).
29. Roberts, N. W., Chiou, T-H., Marshall, N. J. & Cronin, T. W. A biological quarter-wave retarder with excellent achromaticity in the visible wavelength region. *Nature Photon.* **3,** 641–644 (2009).
30. Jen, Y-J. *et al.* Biologically inspired achromatic waveplates for visible light. *Nature Commun.* **2,** 363 (2011).
31. Roberts, N. W., Porter, M. L. & Cronin, T. W. The molecular basis of mechanisms underlying polarization vision. *Phil. Trans. R. Soc. B* **366,** 27–37 (2011).
32. Temple, S. E. *et al.* High-resolution polarization vision in a cuttlefish. *Curr. Biol.* **22,** R121–R122 (2012).
33. Cronin, T. & Shashar, N. The linearly polarized light field in clear, tropical marine waters: spatial and temporal variation of light intensity, degree of polarization and e-vector angle. *J. Exp. Biol.* **204,** 2461–2467 (2001).
34. Mäthger, L. M., Denton, E. J., Marshall, N. J. & Hanlon, R. T. Mechanisms and behavioural functions of structural coloration in cephalopods. *J. R. Soc. Interface* **6** (suppl 2), S149–S163 (2009).
35. Dacke, M., Nilsson, D., Warrant, E. J., Blest, A. D. & Land, M. F. Built-in polarizers form part of a compass organ in spiders. *Nature* **401,** 470–473 (1999).
36. Colomb, T. *et al.* Polarization imaging by use of digital holography. *Appl. Opt.* **41,** 27–37 (2002).

Acknowledgements

The authors acknowledge support from the Biotechnology and Biological Sciences Research Council (NWR – grant no. BB/G022917/1 and BB/H01635X/1), the Engineering and Physical Sciences Research Council (TMJ – grant no. EP/E501214/1) and the Air Force Office of Scientific Research (NWR – grant no. FA-9550-09-1-0149). The authors thank J. McGregor and S.E. Temple for valuable discussions and I.C. Cuthill for advice on statistical analyses.

Author contributions

J.C.P. initiated the study. T.M.J and N.W.R. performed the modelling and experiments. All authors interpreted the data and co-authored the paper.

Additional information

Supplementary information is available in the online version of the paper. Reprints and permission information is available online at http://www.nature.com/reprints. Correspondence and requests for materials should be addressed to N.W.R.

Competing financial interests

The authors declare no competing financial interests.